Available online at www.sciencedirect.com

ScienceDirect

Energy Procedia 81 (2015) 836 – 845

Energy Procedia

69th Conference of the Italian Thermal Engineering Association, ATI 2014

CFD characterization of pressure drop and heat transfer inside porous substrates

A. Della Torre[a]*, G. Montenegro[a], A. Onorati[a], G. Tabor[b]

[a]*Politecnico di Milano, Department of Energy, via Lambruschini 4, 20156, Milano, Italy*
[b]*College of Engineering, Mathematics and Physical Sciences (CEMPS), University of Exeter, UK*

Abstract

In this work a combination of micro-CT, image-based modeling and CFD has been applied to investigate the phenomena occurring at the micro-scale level in two different porous substrates: open-cell foams and unstructured filtering media. These substrates are of interest in the internal combustion engine field for application in after-treatment systems. Open-cell foams allow achieving a higher ratio between reactants conversion and pressure drop across the catalyst. compared to traditional honeycombs. On the other hand, unstructured filtering media, made of cordierite or SiC, are commonly applied for the manufacturing of Diesel Particulate Filters. Micro-CT technology was adopted to reconstruct the actual microstructure of the porous media, allowing to characterize its main geometrical properties and to generate a computational mesh for CFD simulations. A CFD investigation pointed out how the microscopic geometry influences the pressure drop under different flow conditions. Moreover, a conjugate heat transfer model is applied for investigating the convection between the fluid and the solid. The aim of this analysis is to enhance the understanding of the phenomena occurring at the micro-scale in order to extract useful information for the optimization of the properties of the substrates to be applied in after-treatment devices.

Peer-review under responsibility of the Scientific Committee of ATI 2014

Keywords: open-cellfoam, pressure drop, CFD, turbulence, pore size, porosity

1. Introduction

CFD is a valuable tool for understanding the physics, since it gives an insight into details of the flow, which are difficult to obtain experimentally. In this way, when CFD is applied along with experimental measurements, it

* Corresponding author. Tel.: +39 02 23998631.
E-mail address: augusto.dellatorre@polimi.it

Peer-review under responsibility of the Scientific Committee of ATI 2014
doi:10.1016/j.egypro.2015.12.093

contributes to explain the results and, on the other hand, allows addressing sensitivity analysis on a wide range of parameters. Therefore, an experimentally validated CFD model can be adopted for the characterization of the fluid dynamics and heat-transfer properties of the configuration under different conditions, investigating the effect of a wide range of parameters and providing optimization guidelines.

With specific regard to the characterization of the flow through porous media, some examples of CFD analysis can be found in the literature. In this framework, the modeling of the complex micro-structural geometry represents a particularly challenging task. To overcome this problem, the most of the works [1, 2, 3] resort to an idealized periodic structure (e.g. Kelvin-cell), generated in order to match specific global parameters such as the porosity or the averaged dimensions of pores and struts. On the other hand, a more sophisticated approach consists of adopting X-ray computed tomography (micro-CT) [4, 5, 6, 7] to record the foam microstructure, using suitable techniques [8] for the generation of the geometry and the computational mesh from the scanned images.

In this work, a combination of micro-CT, image-based modeling and CFD will be applied to the characterization of the fluid dynamics and heat-transfer properties of different porous substrates. The aim of the analysis is to investigate the phenomena occurring at the micro-scale of the media, in order to understand how the different microstructures influences the behavior in terms of macro-scale properties. The pressure drop and heat-transfer performances of the samples are compared, explaining their dependency on the morphology of the substrate.

2. The samples

The present analysis will be focused on three representative porous media, which are made of different materials and are characterized by different micro-structural morphologies and geometric properties. The first sample is an Al-alloy open-cell foam (Figure 1a)), exhibiting a 95% porosity and a 40 ppi pore density. The second is an open-cell foam made of silicon carbide (Figure 1b)), having a lower porosity (87%) and a lower pore density (10 ppi) with respect to the Al foam. The third sample differs from the other two for both morphology and material. As matter of the fact, this is a generic unstructured filtering media, adopted for the manufacture of the porous wall of Diesel Particulate Filter (Figure 1c)). It is made of cordierite and is characterized by a 50% porosity and a 16 μm pore size.

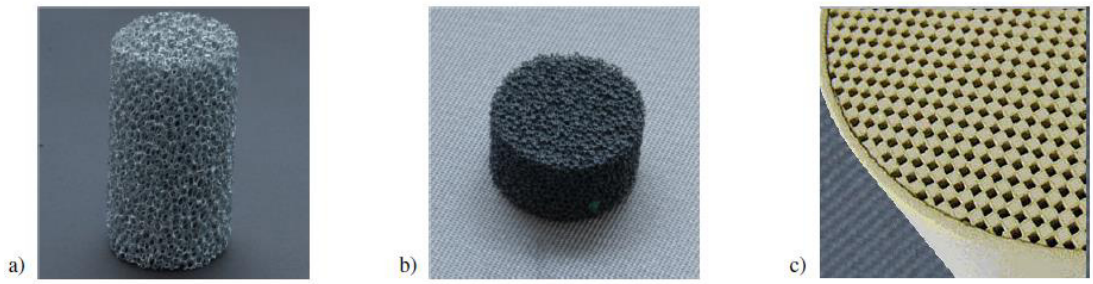

Fig. 1. The samples: a) Al foam, b) SiC foam and c) cordierite filtering media.

3. CFD Modeling

The first step of the CFD modeling consisted of the reconstruction of the micro-structure of the porous media in order to define the geometry of the computational domain. For this operation, an approach based on the combination of X-ray computed tomography (Micro-CT) and Image Based Meshing (IBM) [4, 5] was adopted. These techniques are quite general and can be applied in different fields, some examples can be found in literature related to biomedical applications [9], simulation of flow in packed beds [10] or open- cell foams [4, 7]. A micro-CT scanner operates with a X-ray cone beam which passes through the sample and is collected by a detector. The sample is rotated providing a series of 2D projection images at different angles. A 3D voxel dataset is then reconstructed from the stack of 2D images using inverse methods. In the present work, a Nikon Metrology Benchtop 160 micro-CT system was used for the scanning of the samples; this uses an electron gun operating at up to 160 keV and a metal target to generate a cone of X-rays through bremsstrahlung; both the electron gun voltage and target metal can be

altered to provide a range of spectra and penetration suitable for imaging a range of material compositions from soft biological samples to metal composites. As second step, Image Based Meshing technique was applied, in order to extract a 3D surface model from the voxel dataset; to this purpose the software ScanIP (Simpleware Ltd) has been used. The IBM software operates on the voxel dataset in order to allocate each voxel to fluid or solid matrix region. This process is defined segmentation and can be based on different algorithms; in this work an algorithm based on the definition of a threshold value on the image gray-scale was adopted. As pointed out in [7], the segmentation process is not unique because the correct threshold value on the gray scale of the image for the transition between solid and fluid is not known *a priori*. However, in this work, this issue was overcome choosing the threshold value in such a way that the porosity of the reconstructed micro-structure matches the actual value of porosity experimentally measured. Having segmented the voxel dataset, the Marching Cubes algorithm is applied in order to generate a surface geometry of the micro-structure which can be exported as an *stl* file. Figures 2a)-2c) show the 3D reconstruction of the micro-structural geometry of the three porous media considered in this study.

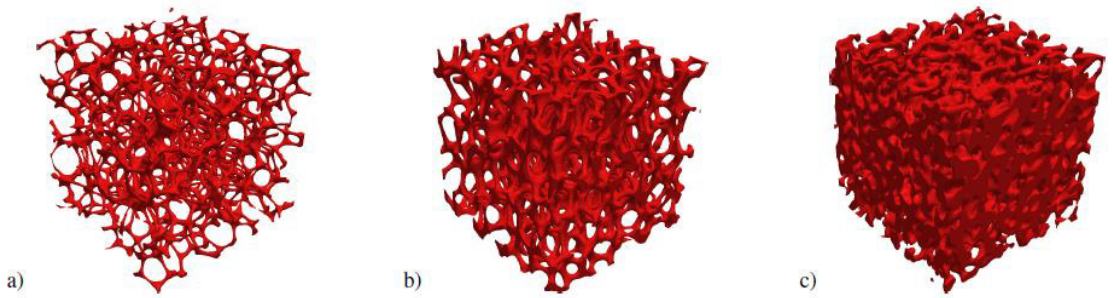

Fig. 2. 3D reconstruction of the micro-structure: a) Al foam, b) SiC foam and c) cordierite filtering media

3.1. Mesh generation

The computational mesh was then generated starting from the STL geometry files, generated by the segmentation software. For the meshing process a cartesian mesh generator (*snappyHexMesh*, a utility included in the open-source CFD toolbox OpenFOAM-2.1.x [11]) was adopted. This is based on the octree concept, where each cell is halved in the proximity of the boundaries, refining the mesh up to the sufficient level. In a first stage, the castellated mesh approximates the shape of the foam in a stair-step way. Then vertices are moved to the nearest boundaries by means of a smoothing algorithm (*snapping phase*). The mesh generated adopting this strategy is predominantly hexahedral, with a small percentage of polyhedral elements near the boundary walls, as shown in Figure 3. The mesh density was chosen by conducting a sensitivity analysis, in order to guarantee the independence of the CFD solution from the grid size.

3.2. Governing equations and numerical setup

Numerical simulations were performed using the open-source OpenFOAM-2.1.x CFD software package [12], which is based on the finite volume approach [13] for the discretization of the governing equations. The computational model is based on the formulation of the conservation equations for the generic continuum, which, combined with the constitutive relations describing the properties of the specific medium (gas, liquid or solid), allows describing the fluid dynamics and heat-transfer phenomena. In particular, considering a Newtonian compressible single-phase fluid, the mathematical set of governing equations consists of:

• Continuity equation, which states the conservation of mass:

$$\frac{\partial \rho}{\partial t} + \nabla(\rho \mathbf{U}) = 0 \tag{1}$$

• Navier-Stokes equation, derived from the conservation of momentum (linear and angular):

$$\frac{\partial \rho \mathbf{U}}{\partial t} + \nabla(\rho \mathbf{U}\mathbf{U}) = -\nabla\left(p + \frac{2}{3}\mu \nabla \cdot \mathbf{U} \right) + \nabla \cdot \left[\mu \left(\nabla \mathbf{U} + \nabla \mathbf{U}^{\mathrm{T}} \right) \right] \quad (2)$$

• Energy equation:

$$\frac{\partial \rho e}{\partial t} + \nabla(\rho e \mathbf{U}) = -\nabla \cdot (p\mathbf{U}) - \nabla \cdot \left[\frac{2}{3}\mu(\nabla \cdot \mathbf{U})\mathbf{U} \right] + \nabla \cdot \left[\mu \left(\nabla \mathbf{U} + \nabla \mathbf{U}^{\mathrm{T}} \right) \mathbf{U} \right] + \nabla \cdot (\lambda \nabla T) + \rho Q \quad (3)$$

This set of equations is closed by means of the perfect gas equation of state. On the other hand, when a solid medium is considered, the set of governing equations reduces to the energy conservation equation, which describes the conductive heat-transfer process:

$$\frac{\partial \rho c_s T}{\partial t} = \lambda_s \nabla T + \rho Q \quad (4)$$

The simulation of the conjugate heat-transfer between fluid and solid phases was addressed considering the full set of equations 1-4, describing the flow of a compressible fluid and the heat-conduction in a solid. In this case, a multi-region framework is required, adopting different computational grids for the solution of the governing equations relative to the fluid and the solid media. The boundary of the two grids coincides at the interface between the regions, as shown in Figure 3.

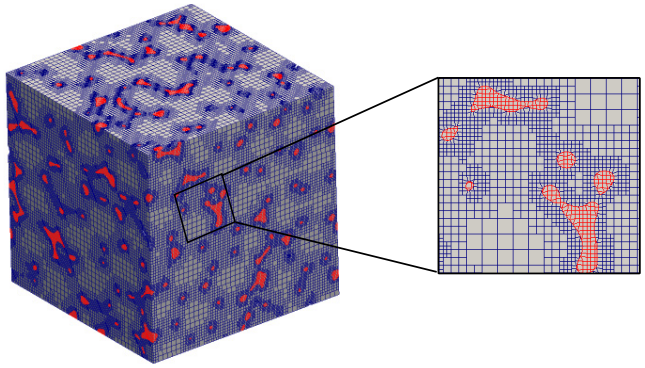

Fig. 3. Mesh for the fluid (blue) and solid (red) regions.

The energy equations, solved on both the fluid and on the solid computational domains, are coupled by means of the heat flux at the interface of the two regions. The steady-state solution of the problem was obtained by applying the SIMPLE algorithm to solve the fluid-dynamics. Moreover, since the characteristic time associated to the conductive heat transfer in the solid is sensibly higher than that one of the fluid-dynamics, a suitable strategy has been implemented in order to speed-up the convergency towards the steady solution. In particular, for each solution iteration performed on the fluid domain, more iterations were performed on the solid one (around 10). A second order upwind scheme (linear upwind) was adopted for the discretization of the convective terms. With regards to the turbulence modeling, simulations were run both in the laminar case or applying the low-Re $k - \omega SST$ model proposed by Menter [14]. No significant differences were found between the two cases, as already reported in [7]. This is due to the fact that, at the flow regimes in which turbulence appears, inertial effects dominate the flow inside the porous matrix, while the viscous effects play a minor role. This means that, with regards to the pressure drop,

this is mainly determined by the inertial contribution and is not significantly affected by the turbulence. On the other hand, also the heat-transfer is not influenced by the turbulence, since it depends mainly on the structure-induced mixing which makes the enhancement of the convective transport promoted by the turbulence negligible. On the other hand, the computational model for the simulation of the conductive heat-transfer inside the solid matrix was based on the solution of the energy equation for the solid phase (Eqn. 4). In this case, the Laplace equation was solved iteratively until convergence was reached.

4. Results and Discussion

The CFD model was applied in order to characterize the fluid-dynamic and heat-transfer properties of the different porous substrates. As first step, simulations of the conductive heat-transfer inside the porous solid matrix were run, evaluating their macroscopic thermal conductivity. Then, conjugate heat-transfer simulations, involving the coupled solution of the governing equations for both the fluid and the solid phases, were applied, characterizing both the permeability and the convection properties of the media under different flow regimes.

4.1. Conductive heat-transfer simulations on single solid phase

Conductive heat-transfer simulations were run imposing different temperatures at the boundary of the sample. Three different orthogonal directions were considered, in order to investigate the effects of the anisotropy of the micro-structure. In Figures 4a), 4b) and 4c) the temperature field in the porous matrix of the Al-foam, the SiC-foam and the cordierite filtering media are shown. In this case a boundary temperature of 800 K was imposed at the hot side while 300 K at the cold one.

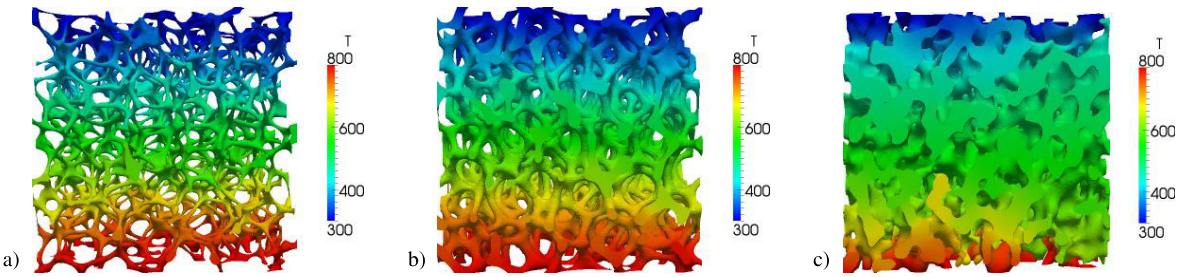

Fig. 4. Temperature field in the solid matrix: a) Al foam, b) SiC foam and c) cordierite filtering media.

From the calculated value of the heat transferred by conduction through the sample the effective conductivity of the porous media can be determined as:

$$\lambda_{eff} = \frac{Q_{cond}}{A(T_h - T_c)} \tag{5}$$

where A is the cross section of the sample. In Figure 5 the bar chart shows the computed conductivity for the three samples, considering the direction of the three coordinate axes x, y, z.

The comparison reveals that the SiC foam exhibits the higher effective conductivity. As matter of the fact, if compared with Al foam, SiC foam is characterized by an higher thermal conductivity of the base material (silicon carbide: $270 W/(mK)$, aluminium: $218 W/(mK)$) and a lower relative density of the foam matrix (SiC foam: 13%, Al foam: 5%). On the other hand, cordierite filtering media, despite the higher relative density (50%), exhibits the lower effective conductivity, due to the very low thermal conductivity of the base material ($2 W/(mK)$). Moreover, for both Al and SiC foams, it can be noticed that the effective conductivity is higher in a certain direction (z-axis for Al foam, y-axis for SiC foam) while similar values are computed in the other two. This can be explained as a consequence of

the manufacture process, which determine slightly different cell geometry in one preferential direction. This can be related to various factors, for instance the presence of the gravitational force, whose nature is clearly directional.

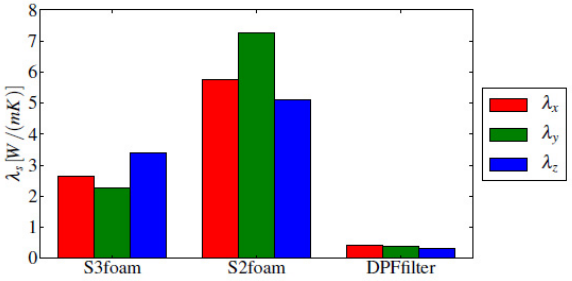

Fig. 5. Effective conductivity of the solid matrices computed for the Al foam, SiC foam and the cordierite filtering media.

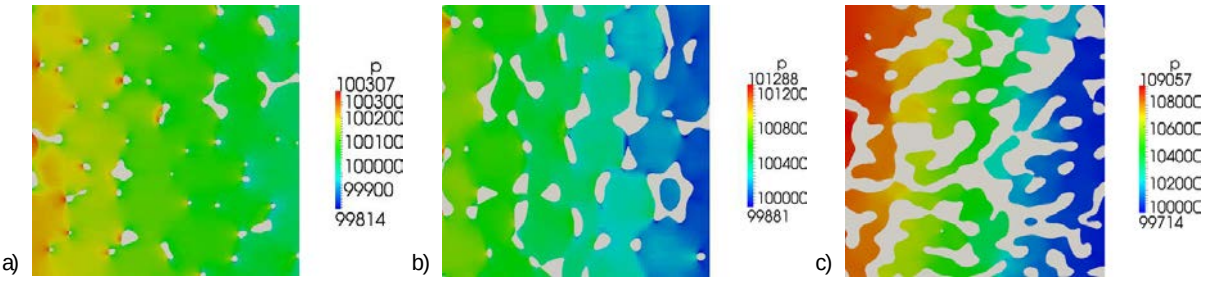

Fig. 6. Pressure field: a) Al foam, b) SiC foam and c) cordietite filtering media.

4.2. Conjugate heat-transfer simulation between fluid and solid phase

Simulations of each sample were run considering a wide range of flow velocities and examining three different operating conditions:

- heating mode: inlet fluid temperature $T_f = 300K$, temperature at the boundary of the solid matrix fixed at $T_s = 500K$;
- cooling mode: inlet fluid temperature $T_f = 500K$, temperature at the boundary of the solid matrix fixed at $T_s = 300K$;
- isothermal mode: inlet fluid temperature equal to the temperature at the boundary of the solid matrix ($T_f = 300K$ and $T_s = 300K$).

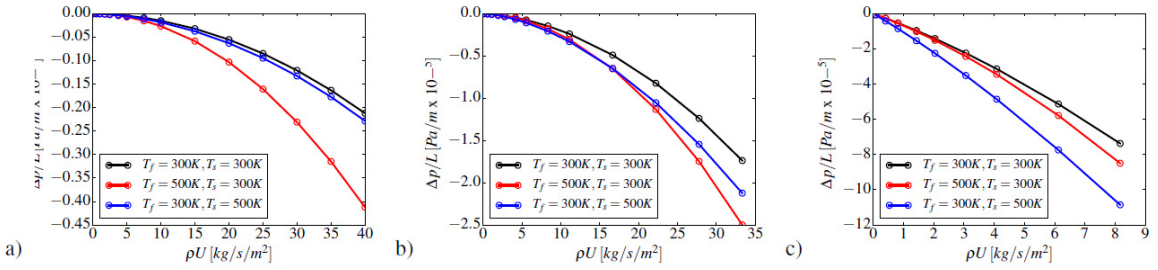

Fig. 7. Pressure gradient across the sample: a) Al foam, b) SiC foam and c) cordierite.

Figures 6 shows, for a cooling situation, the pressure field computed over the fluid domain for the three samples. The pressure gradient across the samples is plotted in Figures 7 as a function of ρU (mass flow divided by the cross-sectional area), considering three different thermal conditions. It can be seen that the

Al foam exhibits the highest permeability, as a consequence of the higher porosity and lower pore density. The pressure gradient becomes one order of magnitude higher in case of the SiC sample and two order of magnitude in case of the cordierite filter. The very low permeability of this filtering media makes it difficult, in practical applications, to use it with high velocity flows, so the simulations were limited to $\rho U = 8\ kg/(s\ m^2)$ (around 10 m/s velocity for an ambient temperature flow).

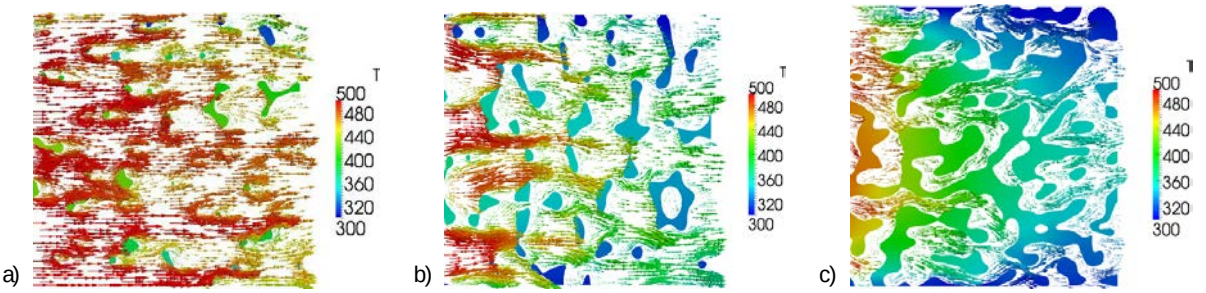

Fig. 8. Temperature field in the solid matrix and velocity vectors colored by the fluid temperature: a) Al foam, b) SiC foam and c) cordierite .

In Figure 8, the temperature field in the solid phase and the fluid velocity vectors, colored by the temperature, are reported. Figures 9 illustrate the dependence of the flow temperature difference between outlet and inlet for different flow condition. With regards to Al foam, it can be seen that, when the mass flow become considerable, the cooling or heating effects tends to become negligible, leading to small temperature differences across the foam. On the other hand, the cordierite substrate is very effective from a heat-exchange point of view, due to its high surface density, heating or cooling the flow to a temperature very closed to the substrate one, even in case of high mass flow. The heat transfer properties of the Si-C foam are in-between with respect to these two extrema, leading to a difference between inlet and outlet fluid temperatures around 100K for the larger mass flow considered.

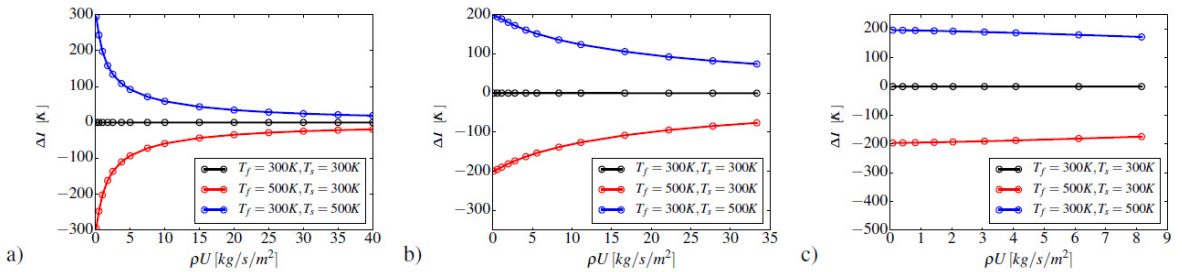

Fig. 9. Temperature difference between inlet and outlet: a) Al foam, b) SiC foam and c) cordierite.

It is interesting to notice the influence of the thermal condition on the pressure drop. For all the three sample the lower pressure drop is obtained for an isothermal condition, while, in presence of heat-transfer with the porous matrix the pressure drop increase. This is due to the fact that, in non-isothermal conditions, the average temperature of the flow is higher than in the isothermal one: this means lower density of the fluid and therefore higher velocity of the flow, resulting in a higher inertial contribution to the pressure drop (Forchheimer term, which has a quadratic dependence on the velocity). Moreover, the maximum pressure drop is obtained in cooling or in heating conditions depending on the sample considered: this is related to the average temperature level of the flow and depends on the heat-transfer properties of the media. For example, for the Al foam the cooling or heating effects tends to become negligible at high mass flow, leading to small temperature differences across the foam. In this case, the average flow temperature is close to the inlet value and therefore the pressure drop is higher in cooling conditions. On the other

hand, for the cordierite filter, the heat transfer is very efficient; therefore the pressure drop is higher in a heating situation, when the flow has a high temperature level.

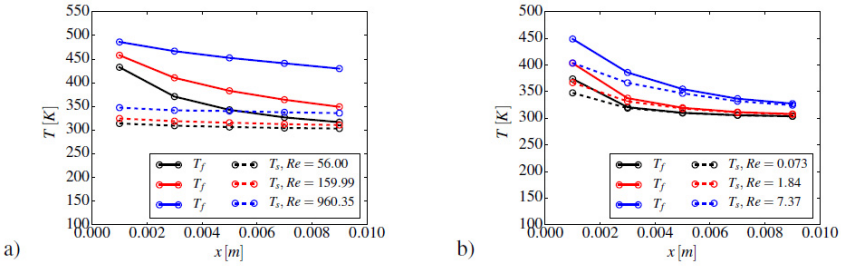

Fig. 10. Temperature profiles of the fluid and solid phases: a) SiC foam and b) cordierite filtering media.

Finally, in Figures 10a) and 10b), the temperature profiles along the axial coordinate are plotted for both the cases of SiC foam and cordierite filtering media, considering different Reynolds numbers. At the high Reynolds numbers, the difference between the fluid and solid phases temperature is considerable. When low Reynolds numbers are considered, the temperature difference between the two phases becomes negligible. This is because, at low Re, the characteristic time of the fluid dynamics tends to become similar to the one of the conductive heat-transfer in the solid phase: the two phases tend therefore to the thermal equilibrium.

The pressure drop predicted by the conjugate heat transfer simulations were analyzed in non-dimensional terms, introducing the Π_1 coefficient according the formulation proposed in [7]:

$$\Pi = \frac{\Delta p d_c^2}{L U_D \mu} = F_1\left(\mathrm{Re} = \frac{\rho U_D d_c}{\mu}\right). \tag{5}$$

If the Darcy-Forchheimer regime is considered, the Darcy-Forchheimer law can be recovered by expressing the functional dependency $F_1(Re)$ as:

$$F_1(\mathrm{Re}) = A + B(\mathrm{Re}), \tag{6}$$

where, $A = d_c^2 / K$, $B = C\, d_c$, K is the permeability and C the form coefficient. In the framework of the Darcy-Forchheimer regime the coefficient A can be seen as the inverse of a non-dimensional permeability coefficient κ:

$$K = \frac{d_c^2}{A} = \kappa d_c^2, \quad \kappa = \frac{1}{A}. \tag{7}$$

If the analysis is extended beyond the limits of the Forchheimer regime, passing to the fully-turbulent regime, the relationship 6 remains still valid, but with different values of the coefficients with respect to Eqn. 7:

$$F_{1,turb}(\mathrm{Re}) = A_{turb} + B_{turb}(\mathrm{Re}), \tag{8}$$

In Figure 11 the non-dimensional Π_1 coefficient is plotted for the cases of the Al foam, the SiC foam and the porous filtering media. It can be noticed that Al and SiC foams exhibits similar relationships between Π_1 and *Re*, showing a change in the slope around *Re* = 250, in correspondence to the transition from laminar Darcy-Forchheimer regime to fully turbulent regime. On the other hand, this cannot be recognized in the relationship for the porous filtering media, since, due to its specific geometrical features, the range of possible regimes is limited to very low

Reynolds numbers. The Π_1 relationships tend to converge to the same line for both isothermal and non-isothermal conditions; the slight difference between heating and cooling modes is due to the different temperature distribution inside the flow field, which determines a different inertial contribution. Moreover, looking at the slope of the lines, it can be argued that the SiC foam gives the highest Forchheimer (inertial) contribution to the pressure drop. On the other hand, the cordierite filter, which operates in Darcy regime (Re < 10), is characterized by the major viscous contribution.

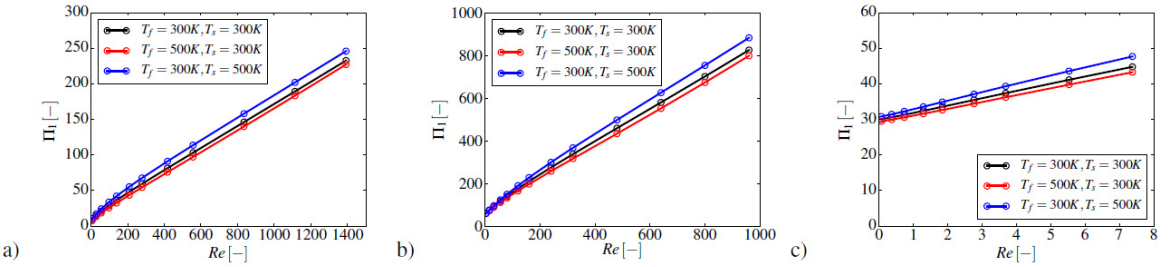

Fig. 11. Dependence of Π_1 coefficient on Re number, considering different temperature of the inlet flow and at the boundary of the solid matrix: a) Al foam, b) SiC foam and c) cordierite filtering media.

5. Conclusions

In this work three different samples were analyzed in order to compare their pressure drop and heat- transfer performances. Micro-CT techniques were applied for the reconstruction of the micro-structural geometry of the sample. The CFD analysis was carried out adopting a multi-region framework, in which two computational grids are applied for the solution of the governing equations for the fluid and the solid media. The conjugate heat-transfer between fluid and solid phases is described coupling interface of the two regions. The analysis showed that the permeability of the media is strictly dependent on their porosity and specific surface. In particular, the Al foam, which has the higher porosity and the lower pore density, exhibits the the solution of the energy equation solved on the two meshes, in order to take into account the heat flux occurring at the lowest pressure drop while the cordierite filter is characterized by the highest resistance to the flow. The introduction of a non-dimensional analysis, allowed us to highlight that the geometrical parameters of the microstructure determines also the flow regime in which the substrate operates under typical conditions. For example, the cordierite filter mainly operates in a Darcy regime, due to the small pore size of the substrate, giving a pressure drop, which depends linearly on the velocity. On the other hand, the regime for Al and SiC foams can range from the Darcy to the fully turbulent one. In addition, the viscous and the inertial contribution changes on the basis of the micro-structural geometric properties: compared to the Al foam, the SiC foam exhibits higher Darcy coefficient, due to the higher surface density, and higher Forchheimer coefficient, due to the lower porosity. With regards to the conductivity of the porous matrix, it has been found that the heat-transfer is determined by the combination of the conductivity of the material and the porosity of the matrix: in the calculation, the best compromise between these factors has been found in case of the SiC foam. On the other hand, the convective heat-transfer is enhanced by the specific surface of the substrate, as in the case of the cordierite filter.

6. Acknowledgments

The authors gratefully acknowledge financial support from the Italian Ministry of Education, University and Research, Rome (MIUR, Progetti di Ricerca Scientifica di Rilevante Interesse Nazionale, prot. 2010XFT2BB), within the project IFOAMS: Intensification of Catalytic Processes for Clean Energy, Low- Emission Transport and Sustainable Chemistry using Open-Cell Foams as Novel Advanced Structured Materials.

7. References

[1] Simulations of flow through open cell metal foams using an idealized periodic cell structure, International Journal of Heat and Fluid Flow 24 (6) (2003) 825–834.
[2] S. Krishnan, M. J. Y., S. V. Garimella, Direct Simulation of Transport in Open-Cell Metal Foam, Journal of Heat Transfer 128 (2006) 793–799.
[3] F. Lucci, A. Della Torre, J. von Rickenbach, G. Montenegro, D. Poulikakos, P. Dimopoulos Eggenschwiler, Performance of randomized Kelvin cell structures as catalytic substrates: mass-transfer based analysis, Chemical Engineering Science 112 (0) (2014) 143 – 151.
[4] G. Tabor, O. Yeo, P. Young, P. Laity, CFD Simulation of Flow through an Open Cell Foam, International Journal of Modern Physics Vol. 19 (2008) 703–715.
[5] J.Petrasch, F.Meier, H.Friess, A.Steinfeld, Tomography based determination of permeability, Dupuit-Forchheimer coefficient, and interfacial heat transfer coefficient in reticulate porous ceramics, Mechanics of Materials Vol. 29 (2008) 315–326.
[6] An appraisal of the heat transfer properties of metallic open-cell foams for strongly exo-/endo-thermic catalytic processes in tubular reactors, Chemical Engineering Journal 198-199 (0) (2012) 512 – 528.
[7] A. Della Torre, G. Montenegro, G. Tabor, M. Wears, CFD characterization of flow regimes inside open cell foam substrates, International Journal of Heat and Fluid Flow 50 (0) (2014) 72 – 82.
[8] P. Young, T. B. H. Beresford-West, S. R. L. Coward, B. Notarberardino, B. Walker, A. Abdul-Aziz, An efficient approach to converting computational models three-dimensional image data into highly accurate computational models, Philosophical Transaction of The Royal Society A Vol. 366 (2008) 3155–3173.
[9] B. Notarberardino, P. G. Young, G. R. Tabor, L. Hao, I. G. Turner, A. Harkara, Structural and Fluid Transport Characterization of Bio-scaffolds based on 3D Imaging Data, International conference on Biomedical and Pharmaceutical Engineering.
[10] M. J. Baker, P. G. Young, G. R. Tabor, Image based meshing of packed beds of cylinders at low aspect ratios using 3d MRI coupled with computational fluid dynamics, Computers and Chemical Engineering Vol. 35 (No. 10) (2011) 1969–1977.
[11] OpenFOAM documentation, Avaiable from: http://www.openfoam.org/docs/.
[12] H. G. Weller, G. Tabor, H. Jasak, C. Fureby, A Tensorial Approach to CFD using Object Orientated Techniques, Computers in Physics Vol. 12 (No. 6) (1998) 620.
[13] H. K. Versteeg, W. Malalasekera, An introduction to computational fluid dynamics, Longman Scientific&Technical,1995.
[14] F. Menter, T. Esch, Elements of Industrial Heat Transfer Prediction, 16th Brazilian Congress of Mechanical Engineering (COBEM).